Fully Synthetic Injectable Depots With High Drug Content and Tunable Pharmacokinetics for Long-Acting Drug Delivery

Duy-Khiet Ho[1,‡], Clare LeGuyader[1,‡], Selvi Srinivasan[1], Debashish Roy[1], Vladimir Vlaskin[1], Thomas E. J. Chavas[1], Ciana L Lopez[1], Jessica M Snyder[2], Almar Postma[3], John Chiefari[3], Patrick Stayton[1,*]

[1]Department of Bioengineering, University of Washington, Seattle, Washington 98195, United States

[2]Department of Comparative Medicine, School of Medicine, University of Washington, Seattle, Washington 98195, United States

[3]CSIRO Manufacturing, Bag 10, Clayton South MDC, Victoria 3169, Australia

[‡]These authors contributed equally to this paper and should be considered equal co-first authors.

*Correspondence to:

Patrick Stayton, Ph.D.

Professor

Box 355061, Department of Bioengineering, University of Washington

Seattle, WA 98195, stayton@uw.edu

Keywords: Long-acting depot, HIV, TAF, pre-exposure prophylaxis, polymer, drug delivery, RAFT, infectious disease

Abstract

Clinical studies have validated that antiretroviral (ARV) drugs can serve as an HIV pre-exposure prophylactic (PrEP) strategy. Dosing adherence remains a crucial factor determining the final efficacy outcomes, and both long-acting implants and injectable depot systems are being developed to improve patient adherence. Here, we describe an injectable depot platform that exploits a new mechanism for both formation and controlled release. The depot is a polymeric prodrug synthesized from monomers that incorporate an ARV drug tenofovir alafenamide (TAF) with degradable linkers that can be designed to control release rates. The prodrug monomers are synthetically incorporated into homopolymer or block designs that exhibit high drug weight percent (wt%) and also are hydrophobized in these prodrug segments to drive depot formation upon injection. Drug release converts those monomers to more hydrophilic pendant groups via linker cleavage, and as this drug release proceeds, the polymer chains losing hydrophobicity are then disassociated from the depot and released over time to provide a depot dissolution mechanism. We show that long-acting TAF depots can be designed as block copolymers or as homopolymers. They can also be designed with different linkers, for example with faster or slower degrading *p*-hydroxybenzyloxycarbonyl (Benzyl) and ethyloxycarbonyl (Alkyl) linkers, respectively. Diblock designs of p(glycerolmethacrylate)-*b*-p(Alkyl-TAF-methacrylate) and p(glycerolmethacrylate)-*b*-p(Benzyl-TAF-methacrylate) were first characterized in a mouse subcutaneous injection model. The alkylcarbamate linker design (TAF 51 wt%) showed excellent sustained release profiles of the key metabolite tenofovir (TFV) in skin and plasma over a 50-day period. Next, the homopolymer design with a high TAF drug wt % of 73% was characterized in the same model. The homopolymer depots with p(Alkyl-TAFMA) exhibited sustained TFV and TAF release profiles in skin and blood over 60 days, and TFV-DP concentrations in peripheral blood mononuclear cells (PBMC) were found to be at least 10-fold higher than the clinically suggested minimally EC90 protective concentration of 24 fmol/10^6 cells. These are the first reports of sustained parent TAF dosing observed in mouse and TFV-DP in mouse PBMC. IVIS imaging of rhodamine labeled homopolymer depots showed that degradation and release of the depot coincided with the sustained TAF release. Finally, these homopolymers showed excellent stability in accelerated stability studies over a six-month time period, and exceptional solubility of over 700 mg/mL in the DMSO formulation solvent. The homopolymer designs have a drug reservoir potential of well

over a year at mg/day dosing and may not require cold chain storage for global health and developed world long-acting drug delivery applications.

Abbreviations

Pre-exposure prophylaxis: PrEP
initiative pre-exposure prophylaxis: iPrEx
Antiretroviral: ARV
Tenofovir alafenamide: TAF
Tenofovir: TFV
TFV-diphosphate: TFV-DP
tenofovir disoproxil fumarate: TDF
Emtricitabine: FTC
Long-acting cabotegravir: CAB LA
Long-acting rilpivirine: RPV LA
Poly(lactic-*co*-glycolic acid): PLGA
Pharmacokinetic: PK
Peripheral blood mononuclear cells: PBMC
4-(((2-carboxyethyl)thiocarbonothioyl)thio)-4-cyanopentanoic acid: CCC
4-cyano-4-((ethylsufanylthiocarbonyl)-sulfanyl)pentanoic acid: ECT
Azobisisobutyronitrile: AIBN
2,2'-Azobis(4-methoxy-2,4-dimethylvaleronitrile): V-70
Reversible Addition-Fragmentation Chain Transfer Polymerization: RAFT
Poly(glycerolmethacrylate) macro chain transfer agent: p(GMA) mCTA
Rhodamine B methacrylate: RhMA
Benzyl carbamate TAF methacrylate: Benzyl-TAFMA
Ethyl carbamate TAF methacrylate: Alkyl-TAFMA
p(glycerolmethacrylate)-*b*-p(benzyl carbamate TAF methacrylate): p(GMA)-*b*-p(Benzyl-TAFMA)
p(glycerolmethacrylate)-*b*-p(ethyl carbamate TAF methacrylate-*co*-Rhodamine B methacrylate): p(GMA)-*b*-p(Alkyl-TAFMA-*co*-RhMA) or p(GMA)-*b*-p(Alkyl-TAFMA)
p(benzyl carbamate TAF methacrylate-*co*-Rhodamine B methacrylate): p(Benzyl-TAFMA-*co*-RhMA) or p(Benzyl-TAFMA)
p(ethyl carbamate TAF methacrylate-*co*-Rhodamine B methacrylate): p(Alkyl-TAFMA-*co*-RhMA) or p(Alkyl-TAFMA)
Liquid chromatography method, coupled with tandem triple quadrupole mass spectrometry: LC-MS/MS
Weight percent: wt%
Size Exclusion Chromatography: SEC
Internal standards: IS
para-Hydroxybenzyloxycarbonyl: PHBC
Ethyloxycarbonyl: EC
Mono-2-(methacryloyloxy)ethyl succinate: SMA
N-*N*'-Dicyclohexylcarbodimide: DCC
4-(Dimethylamino)pyridine: DMAP
p-Hydroxybenzyl alcohol: PHB-OH
Molecular weight: MW
Number average molecular weight: M_n
Weight average molecular weight: M_w
Polymerization degree: DP
Chain transfer agent: CTA

1. Introduction

Pre-exposure prophylaxis (PrEP) for HIV prevention has become an important clinical strategy to reduce infection acquisition. The seminal iPrEx trial demonstrated that daily administration of Truvada, an oral combination drug of tenofovir disoproxil fumarate (TDF) and emtricitabine (FTC), reduced HIV transmission. Truvada is now recommended by the CDC and WHO for PrEP in concert with behavioral risk reductions. These critical clinical studies also made clear that PrEP failed to prevent infections when adherence to daily dosing failed.[1–3] The iPrEx trial found that individuals who took pills less than 50% of the prescribed regimen exhibited an 84% chance of HIV infections, and estimated that full adherence would drop acquisition to a remarkable 8% or less. The Partners PrEP trial showed that women taking TDF alone or in combination with FTC exhibited 49-79% reductions in transmission, with greater than 85% reduction in high adherence individuals.[4] The complexities and challenges of PrEP in global settings were also demonstrated in the FEM-PrEP study conducted in Africa.[5] This study was terminated when it was found that there was no significant reduction in HIV incidence because the majority of participants were not adherent. Similarly, the VOICE study in South Africa, Uganda and Zimbabwe found that oral TDF, oral Truvada, or 1% TFV vaginal gel did not reduce rates of HIV acquisition due to low patient dosing adherence.[6] These challenges and requirements have led to a growing interest in long-acting/sustained release drug products for PrEP and therapy.

The current long-acting products under clinical development are generally drug implants or injectable depots.[7–10] The long-acting cabotegravir intramuscular injectable product (CAB LA) has shown exciting recent efficacy in a global randomized, controlled, double-blind study.[11–13] Long-acting rilpivirine (RPV LA) is another injectable formulation that maintains efficacious drug dosing as a monotherapy or in combination with CAB LA.[14–19] Other injectable depots are also under development including nanoparticle formulations,[10,20,21] biodegradable polymer formulations,[22,23] and thermogelling biopolymer-peptide fusions for other chronic disease applications.[24] Long-acting subcutaneous implants have also been studied in phase 1 trials that deliver islatravir dispersed within degradable polycaprolactone or poly(ethylene-vinyl acetate) devices. Initial trial data showed that a 62 mg islatravir implant achieved a linear release of drug and efficacious levels of active metabolite in PBMC over 12 months.[9,25] Similarly, removable and refillable implants for delivering TAF and emtricitabine are under study for long acting (ARV) HIV drug delivery.[8,9,26–30]

Critical attributes for injectable PrEP depot products include longer delivery windows per injection, lower volume to reduce patient injection discomfort, and minimal initial and run-out burst release profiles. We describe here a new long-acting depot platform to address these requirements that is adapted from recently developed polymeric prodrug therapeutics termed "drugamers". Drugs are first synthesized as prodrug vinyl monomers with designable hydrolytic or enzyme-cleavable linkers.[31–34] These prodrug monomers can then be polymerized into a versatile repertoire of depot designs including homopolymers, or as block copolymers such as A-B designs. The polymers deposit as physical gels after injection due to the hydrophobically-driven chain associations in the subcutaneous space. As the linkers cleave and drugs are released from the polymers in the depot, the conversion of those monomers to more hydrophilic pendant groups converts those polymer chains to a more hydrophilic state (**Figure 1**). Polymer chains that have lost critical levels of drug are then released from the depot to provide a dissolution mechanism distinct from the matrix degradation and drug release associated with current biodegradable polymer formulations such as PLGA.[35]

The physical properties of ARV drugs, such as their lipophilicity and crystallinity, can be a challenge for formulation or co-formulation using conventional nanoparticle and microparticle technologies, but become only minimally important in the drugamer formulation approach because the drugs are synthetically conjugated at the prodrug monomer synthesis stage. This drugamer platform also provides control of drug combinations at designable drug ratios, and at significantly higher drug weight percent (wt%) than traditional polymer-drug conjugates and many degradable polymer formulations, by a facile controlled polymerization of the pre-synthesized prodrug monomers.[31,36] The linkers provide an important handle on controlling release profiles and pharmacokinetics (PKs) via the well established library of hydrolytic, redox and enzyme-sensitive linker sets.[31,33,37,38] Finally, the depot is a synthetic polymer product rather than a traditional formulation with favorable CMC and GMP pathways to future clinical development.

TAF has drawn interest for HIV PrEP due to its ability to load the PBMC compartment with the long-lived TFV-diphosphate (TFV-DP) active metabolite that can provide long-acting protection.[39,40] We have developed the chemistry for drugamer depots with TAF and investigated both architecture and linker degradation as tunable handles to control depot deposition, drug loading capacity, and drug release kinetics. While the mouse has been previously described as a model for TAF depot studies,[41,42] important details of TAF metabolism in the

mouse were missing from the literature. We first characterized TAF delivered into the blood from the subcutaneous compartment, including the first demonstration of TAF metabolism and loading of the active TFV-DP metabolite in the mouse peripheral blood mononuclear cells (PBMC) compartment. This PK information was then applied to characterize and develop the TAF drugamer depots that exhibit tunability in release profiles, high drug content up to 73 drug wt %, along with outstanding solubility and injectability properties. The drugamer depots thus appear suited for long-acting injectable depots over time periods ranging from months to years, including global health applications where their stabilization of TAF may reduce the need for cold-chain supply and storage.

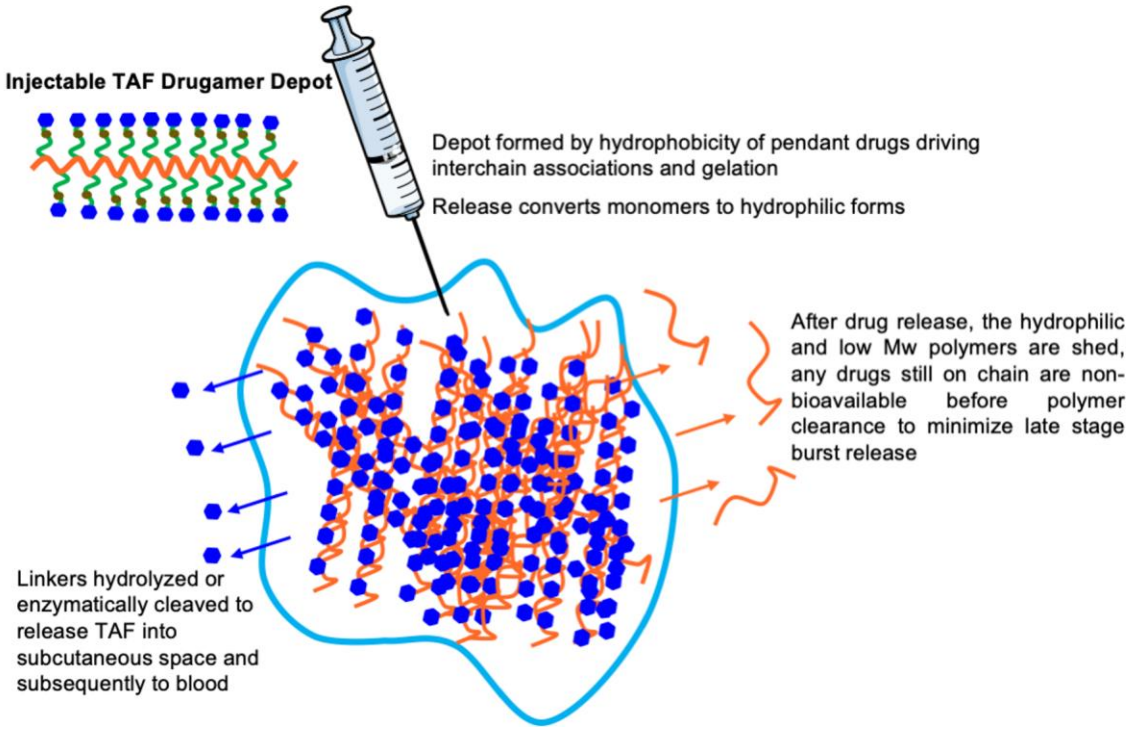

Figure 1. Schematic mechanism for drugamer depot formation and dissolution. The depot is composed simply of the polymer in injection solvent. Drug release is controlled by the linker design in the prodrug monomer units and by the local environment in the depot that controls water and enzyme access to the degradable linker atoms. Drug release and ester hydrolysis leave hydrophilic pendant groups that switch chains to a hydrophilic, lower MW state that can be shed from the depot. Chains still containing drugs are expected to clear with faster relative kinetics than the drug cleavage itself, providing a mechanism to reduce end-stage burst release.

2. Materials and experimental methods

2.1. Materials

Materials were purchased from Sigma-Aldrich unless otherwise specified. All solvents were Fisher HPLC grade. Chain transfer agents, 4-(((2-carboxyethyl)thiocarbonothioyl)thio)-4-cyanopentanoic acid (CCC) and 4-cyano-4-((ethylsufanylthiocarbonyl)-sulfanyl)pentanoic acid (ECT) were purchased from Boron Molecular and OMM Scientific (Texas, USA), respectively. Glycerol monomethacrylate was purchased from Polysciences and purified using basic alumina before polymerization. 2,2'-Azobis(4-methoxy-2,4-dimethylvaleronitrile) (V-70) was purchased from FUJIFILM Wako Pure Chemical Corporation, USA and used without further purification. Fasudil hydrochloride was purchased from eNovation Chemicals (Green Brook, NJ, USA). Spectra/Por regenerated cellulose dialysis membranes were purchased from Spectrum Laboratories (Houston, TX, USA). Rhodamine B methacrylate (RhMA) was synthesized as described previously.[43] Tenofovir alafenamide (TAF) fumarate (1:1 salt) was obtained from MedKoo Biosciences, Inc. Analytical standards: tenofovir (TFV) and tenofovir diphosphate (TFV-DP) were obtained from Cayman Chemical and Santa Cruz Biotech, respectively. Isotopic internal standards: TAF-d_5 fumarate, TFV-d_6 and TFV-DP $^{13}C_5$ were obtained from Toronto Research Chemicals and Moravek, respectively. HPLC grade methanol and water were purchased from VWR international Ltd.

2.2. Synthesis of TAF prodrug monomers

Synthetic **Scheme S1A** and **Scheme S2** in the supporting information were followed to obtain *p*-hydroxybenzyloxycarbonyl TAF methacrylate (Benzyl-TAFMA, monomer **6**) and ethyloxycarbonyl TAF methacrylate (Alkyl-TAFMA, monomer **10**) monomers, respectively. All the synthesized compounds were purified by precipitation and/or silica gel column chromatography. The successful synthesis and purity of the monomers were confirmed and characterized by ^{1}H NMR spectroscopy (Bruker Avance spectrometers 300 MHz) and Electrospray Ionization-Mass spectrometry (Bruker Esquire ion trap mass spectrometer). The full synthetic procedures and associated characterization data are detailed in the supporting information.

2.3. Synthesis of TAF prodrug polymers

RAFT was used to synthesize poly(glycerol monomethacrylate) macro chain transfer agent (p(GMA) mCTA) and all TAF drugamers, including p(GMA)-*b*-p(Benzyl-TAFMA), p(GMA)-*b*-p(Alkyl-TAFMA-*co*-RhMA), p(Benzyl-TAFMA-*co*-RhMA) and p(Alkyl-TAFMA-*co*-RhMA). The synthesized polymers were characterized by ^{1}H NMR spectroscopy and Size Exclusion

Chromatography (SEC). The full synthetic procedures and associated characterization data are detailed in the supporting information.

2.4. Accelerated storage stability study of p(GMA)-*b*-p(Benzyl-TAFMA)

The diblock p(GMA)-*b*-p(Benzyl-TAFMA) was selected for accelerated stability characterization in the solid state as it contains the less stable, faster degrading linker. The polymer was lyophilized and incubated at 40 ± 2 °C for 6 months (26 weeks) in an open vial in the absence of humidity control. The time points were set as day 0, 7, 14, 21, 28, 42, 56, 70, 98, 126, 154 and 182. For each time point, 15 mg of lyophilized polymer in open 20 mL scintillation vial was placed in an incubator (Fisher Scientific Isotemp incubator) preheated to 40 °C. At the end of each time point, the corresponding polymer sample was removed from the incubator, capped and stored at -20 °C until further analysis. After completion of all time points, the stability was examined by high-performance liquid chromatography (HPLC) with analyte detection achieved by monitoring UV/Vis absorption and ^{1}H NMR spectroscopy. HPLC was run on a Hewlett Packard 1100 liquid chromatograph system with a Brucker Esquire-LC ion trap mass spectrometer. LC separation was carried out using Agilent Zorbax SB-C18, Narrow bore, 2.1 mm x 100 mm, 3.5 Micron (Agilent Technologies) with mobile phase A (94% water + 5% acetonitrile + 1% acetic acid) and mobile phase B (99% acetonitrile + 1% acetic acid). The column and the autosampler were kept at 30 °C and 4 °C, respectively. The flow rate was 0.2 mL/min and the injection volume for each run was 10 µL. The linear gradient was as follows: 0–13 min, 2–60% B linear; 13–15min, 60–95% B linear; holding at 95% B for 2 min; 17–19 min, 95–2% B linear and 4 min post time with 98% mobile phase A to equilibrate the column. UV detection was at 280 nm. The total run time for analysis was 23 min. The percentages of released TAF from the polymer were calculated as equation (I):

$$Released\ TAF\ (\%) = \frac{amount\ of\ released\ TAF}{initial\ amount\ of\ TAF\ in\ polymer}\ \text{x}\ 100 \quad \text{(I)}$$

Whereas: the amount of released TAF was analyzed using HPLC, and the initial amount of TAF in polymer was the equivalent TAF amount in 15 mg of the polymer.

For ^{1}H NMR analysis, the samples were prepared in DMSO-d_6 at a concentration of 10 mg/mL, and the spectra were recorded with 128 scans (Bruker Avance spectrometers 300 MHz).

2.5. Animals procedure and ethics statement

All animal procedures and handling were performed with the approval of the Institutional Animal Care and Use Committee and kept in accordance with federal and state policies on animal research at the University of Washington. Female BALB/cJ mice, aged 6-8 weeks at time of experiments, were obtained from Jackson Laboratory (Bar Harbor, ME). Mice were housed in specific pathogen-free conditions (excluded rodent pathogens include mouse hepatitis virus, mouse parvovirus, minute virus of mice, reovirus-3, pneumonia virus of mice, rotavirus, Theiler mouse encephalomyelitis virus, lymphocytic choriomeningitis virus, ectromelia virus, Sendai virus, *Mycoplasma pulmonis*, and pinworms and fur mites) and maintained in light-dark cycles of 12h with *ad libitum* access to food and water.

At the designated time points, mice were anesthetized with 3% isoflurane. Blood was collected via terminal cardiac puncture and immediately transferred to lithium heparin blood collection tubes (BD) and stored at 4 °C until further processing to collect plasma and to collect PBMC (detailed information is in the supporting information). The skin explant carrying polymer depot was collected and stored at -80 °C until further processing and analysis (detailed information is in the supporting information).

2.6. Metabolism of TAF in mouse model

2.6.1. Metabolism of TAF from intravenous injection

The metabolism of TAF by intravenous (IV) administration was investigated in order to analyze and validate reliable metabolites for the future depot PK studies. TAF was formulated in 5% dextrose at a concentration of 90 mg/mL. The dosing solution of 100 µL was then injected intravenously using 29G × 1/2" (BD) to reach the dose of 45 mg/kg TAF equivalent. Plasma and PBMC were collected at designated time points (5 min, 15 min, 30 min, 1 h, 2 h, 4 h, and 8 h). Concentrations of TAF and its metabolites found in mouse, including TFV-alanine, TFV and TFV-DP, were analyzed. Three mice were included per time point.

2.6.2. Metabolism of TAF from injection in the subcutaneous compartment

Free TAF was dissolved in the mixture of ultrapure water, USP grade propylene glycol and benzyl alcohol (4:5:1 *v/v*) at a concentration of 67.7 mg/mL. The dosing solution of 100 µL was then injected into the subcutaneous space on the flank of mice using 25G × 5/8" needle (BD) to reach the dose of TAF at 6.77 mg/mouse. Plasma and skin were collected at designated time points (5 min, 30 min, 4 h, 2 d, 4 d, 6 d, 8 d and 10 d). Concentrations of TAF and TFV were analyzed.

Three mice were included per time point. PBMC were collected from three mice per time point and combined prior to TFV-DP analysis.

2.7. Characterization of TAF depot sustained release performance

2.7.1. Drugamer depot formulations and injection

The diblock polymers were formulated in a mixed solvent system used in prior FDA-approved products composed of ultrapure water, USP grade propylene glycol and benzyl alcohol (4:5:1 *v/v*), while the homopolymers were formulated in DMSO. The lyophilized polymer was dissolved in the corresponding vehicle to give an injectable solution with low viscosity. Dosing volumes and concentrations were chosen so that the same amount of TAF at 6.77 mg/mouse was injected for each of the polymers studied. The final dosing volumes and concentrations were 100 µL for the p(GMA)-*b*-p(Benzyl-TAFMA) 34 wt% TAF at 200 mg/mL concentration, 100 µL for the p(GMA)-*b*-p(Alkyl-TAFMA) 51 wt% TAF at 133 mg/mL concentration, 20 µL for the p(Benzyl-TAFMA) 54.5 wt% TAF at 625 mg/mL concentration, or 20 µL for the p(Alkyl-TAFMA) 73 wt% TAF at 465 mg/mL concentration. The polymer solutions were injected into the subcutaneous space on the flank of mice using 25G × 5/8" needle (BD). Plasma, PBMC and skin were collected at designated time points. Concentrations of TAF, TFV and TFV-DP were analyzed. Three mice were included per time point.

2.7.2. Safety and tolerability assessment at the depot injection site

The body weight and body temperature of mice received the drugamer depot formulations (as mentioned in section 2.7.1.) were measured over the 60-d period. The body weight and body temperature of mice received vehicle – DMSO or a mixture of ultrapure water, USP grade propylene glycol and benzyl alcohol (4:5:1 *v/v*) – were measured and used as controls. The data are shown in **Figure S15**. The p(Alkyl-TAFMA-*co*-RhMA) was subcutaneously administered at day 0. The mice were kept for 60 days prior to collecting explanted skins carrying the depot. Tissues were washed twice with PBS and then fixed in 10% neutral buffered formalin, paraffin embedded, cross-sectioned at 4–5 µm, and stained with hematoxylin and eosin (H&E). Images of representative lesions were acquired using NIS-Elements BIR 3.2 64-bit and plated in Adobe Photoshop Elements. Image brightness and contrast was adjusted using auto contrast, brightness and levels settings applied to the entire image. Original magnification is stated and a scale bar is placed. Four mice that received the drugamer depot and three control mice that received 20 µL DMSO were analyzed by a board certified veterinary pathologist who was blinded to treatment.

2.7.3. Determination of depot PK by LC-MS/MS analysis

Drug metabolite concentrations in plasma and skin tissues were determined with an analytical liquid chromatography method, coupled with tandem triple quadrupole mass spectrometry (LC-MS/MS, details are described in the supporting information). Calibration standard solutions were prepared using naive plasma or tissue homogenate spiked with known drug standards and isotopic internal standards (IS). Prior to LC-MS/MS analysis both skin homogenates and plasma samples were extracted with methanol to isolate TAF and its metabolite TFV from the majority of the native milieu that has the potential to affect assay performance. Briefly, IS that had previously been thawed and diluted 400-fold into water from the 10 µg/mL primary stocks, were used to generate a room temperature three-fold aqueous dilution of either plasma or skin homogenate matrix. Each sample was then further diluted three-fold with methanol that had been pre-chilled at -20 °C. After a 30 second vortex to yield a homogeneous suspension, each sample was subjected to a centrifugation cycle for 20 min at 4 °C and 16,000 *g*. The supernatant was then diluted three-fold with water, briefly vortexed and subjected to a second round of centrifugation for 10 min at 4 °C and 16,000 *g*. Sufficient amount of the resulting supernatant was then transferred to a glass LC-MS/MS vial and stored at 4 °C until analysis, that was performed the same day.

The calibrators for the assay were obtained following the above procedure with study sample matrix replaced with plasma and skin from TAF/TFV naive subjects, with the analyte added concurrently with the IS at the appropriate concentration. The calibrators were chosen to span 100 ng/mL to 1 ng/mL plasma in both TAF and TFV during plasma analysis. For skin samples, the appropriate calibrator range was 10 ng/g skin to 150 ng/g skin in both TAF and TFV. All dilutions from primary TAF and TFV stocks were performed using 20% *v/v* aqueous methanol.

In order to quantify TFV-DP in PBMC, it was necessary to modify the LC-MS/MS method developed for detection of TAF and TFV in mouse plasma. It was not necessary to change either the column nor the buffers for the new method, however the LC gradient was adjusted to afford good separation between TFV-DP and TFV-d_6 which was used as the IS for the assay. Briefly, isolated PBMC that had been stored at -80 °C in a PBS solution, were thawed, at which point 300 µL portions, each carrying ~75% of the total PBMC quantity from a given subject, were centrifuged for 10 min at 600 *g* and 4 °C, to yield PBMC pellets. To each centrifuge tube containing a PBMC pellet, was added 30 µL methanol containing 10% *v/v* DMSO. All samples were sonicated for 5 min at room temperature, then 10 µL of IS working stock containing 20 ng/mL of TFV-d_6 in

20% *v/v* methanol were added to each tube, followed by another 10 µL of 20% *v/v* methanol. Similarly, to prepare calibrators for the assay, 10 µL of IS working stocks were followed by 10 µL of a given calibrator stock in 20% *v/v* methanol. The calibrator working stocks were prepared at TFV-DP concentrations ranging from 1000 ng/mL to 10 ng/mL. Both calibrators and study samples were briefly vortexed then centrifuged for 20 min and 4 °C at 17,000 *g*. Supernatants from each tube were further diluted, by transferring 40 µL portions of each supernatant into a fresh centrifuge tube previously charged with 20 µL of HPLC grade water. All samples were briefly vortexed then centrifuged for 10 min at 4 °C and 17,000 *g*. Finally, the resulting supernatants were transferred to glass LC-MS/MS vials and stored on ice until analysis.

2.7.4. IVIS imaging and analysis of depot dissolution kinetics

Mice were subcutaneously administered with rhodamine-labelled p(GMA)-*b*-p(Alkyl-TAFMA-*co*-RhMA) 51 wt% TAF or p(Alkyl-TAFMA-*co*-RhMA) 73 wt% TAF and monitored at the corresponding designed time points of PK studies using fluorescent mode at (Ex/Em: 500/620 nm). The fluorescence intensity emitted from the depot in each mouse was subsequently quantified using Xenogen Living Image software. The elimination rate of the polymer depot was estimated based on the percentage of normalized radiant efficiency as calculated in the equation (II) as below.

$$Normalized\ Radient\ Efficiency\ (\%) = \frac{Intensity_{detected} - Intensity_{min}}{Intensity_{max} - Intensity_{min}} \text{x}100 \quad \text{(II)}$$

Whereas: $intensity_{detected}$ is the radiant efficiency detected at designated time points post-injection, $intensity_{min}$ is the radiant efficiency detected in control mice received vehicle, and the $intensity_{max}$ is the radiant efficiency detected right after the depot formation. Selected organs of mice received p(Alkyl-TAFMA-*co*-RhMA), including brain, liver, kidneys, lungs and spleen, were harvested at designated time points and imaged using a fluorescent mode of IVIS (Ex/Em: 530/585 nm) to observe the elimination of the polymer depot. All images were taken using Caliper Xenogen IVIS (PerkinElmer, Hopkinton, MA).

3. Results and Discussion

3.1. Synthesis and characterization of TAF prodrug monomers

The prodrug monomers can be polymerized directly to polymer-drug therapeutics, opening new release tunability, architectural designs, and drug loading levels.[31,44,45] Additionally, the loading of each component can be easily controlled by simple variation of the monomers stoichiometry. The chemical structures of prodrug monomers used in this work, Benzyl-TAFMA

(monomer 6) and Alkyl-TAFMA (monomer 10), are shown in **Figure 2**. Both monomers are composed of three-components: TAF drug, a polymerizable methacrylate moiety, and either the *para*-hydroxybenzyloxycarbonyl (PHBC) or ethyloxycarbonyl (EC) linker. A five-step synthetic route starting from mono-2-(methacryloyloxy)ethyl succinate (SMA) as outlined in **Scheme S1A** was followed to obtain Benzyl-TAFMA. The carboxylic group of SMA was first activated with 2-thiazoline-2-thiol using *N*-*N*′-dicyclohexylcarbodimide (DCC) and 4-(dimethylamino)pyridine (DMAP) and then coupled to *p*-hydroxybenzyl alcohol (PHB-OH) in the presence of DMAP. Acylation predominantly proceeded at the phenolic hydroxyl group as the phenolate anion generated under basic condition is more nucleophilic than the benzylic hydroxyl group, providing SMA-PHBA (3). Phenolic acylation was confirmed by the presence of benzylic hydroxyl signal at 1.75 ppm in ^{1}H NMR spectrum. 1,1′-Carbonyldimidazole was used to convert the benzylic hydroxyl group of 3 into an activated carbonate monomer (4) and this step resulted in a downfield shift of benzylic methylene signal from 4.68 to 5.40 ppm. Attempts to conjugate 4 to the amine group on the purine ring of TAF was unsuccessful. A similar approach with 4-nitrophenyl activated carbonate monomer also failed, indicating that the less nucleophilic purine amine requires a robust acylating reagent for successful conjugation. Hence, a highly reactive *N*-methylimidazolium triflate quaternized salt monomer was prepared by reacting 4 with methyl trifluoromethanesulfonate following the methods developed by Rapoport *et al.*[46,47] This reactive intermediate 5 underwent the coupling successfully providing Benzyl-TAFMA (monomer 6) in 84 % yield. The successful conjugation was confirmed by the carbamate NH signal at 10.64 ppm and an upfield shift of benzylic methylene group from 5.40 to 5.21 ppm in ^{1}H NMR spectrum. TAF purine protons appeared at 8.41 and 8.61 ppm and isopropyl moiety signals were observed at 1.14 and 4.84 ppm. The self-immolative property of the spacer PHBC in Benzyl-TAFMA is well known. The phenolic ester linkage is cleaved leading to a cascade of chemical reactions that triggers the release of TAF as shown in **Scheme S1B**.[48,49] Alkyl-TAFMA was prepared using the same activation strategy described above and the synthetic steps are outlined in **Scheme S2**.

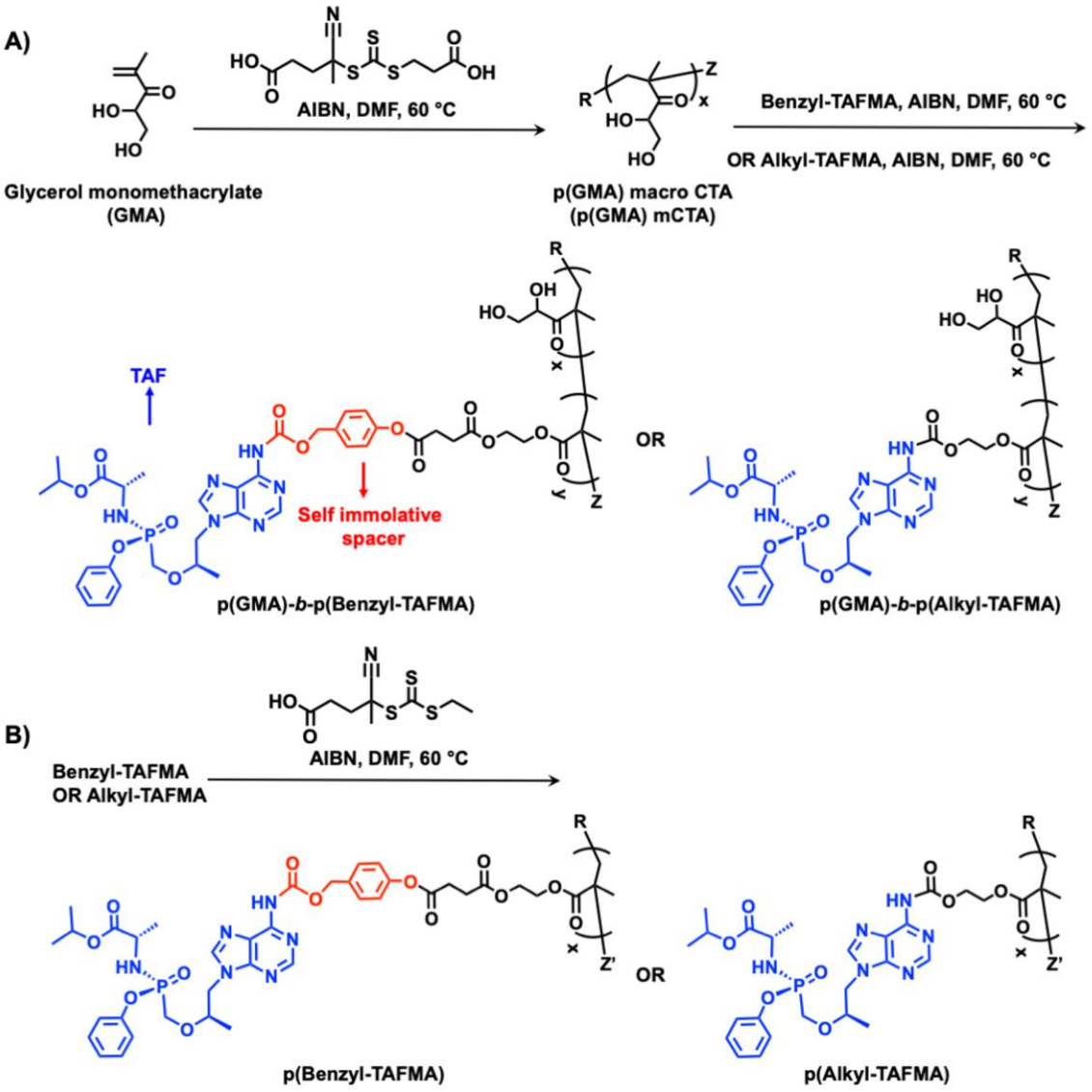

Figure 2. (**A**) Schematic synthesis of p(GMA) mCTA with subsequent diblock synthesis to final p(GMA)-*b*-p(Benzyl-TAFMA) or p(GMA)-*b*-p(Alkyl-TAFMA); the structures of Benzyl-TAFMA and Alkyl-TAFMA monomers with TAF drug and *para*-hydroxybenzyloxycarbonyl (PHBC) or ethyloxycarbonyl (EC) spacer are also illustrated. (**B**) Homo-polymerization to produce p(Benzyl-TAFMA) and p(Alkyl-TAFMA).

3.2. Synthesis and characterization of TAF drugamers

3.2.1. Synthesis of diblock TAF drugamers: p(GMA)-*b*-p(Benzyl-TAFMA) and p(GMA)-*b*-p(Alkyl-TAFMA-*co*-RhMA)

The amphiphilic diblock drugamers – p(GMA)-*b*-p(Benzyl-TAFMA) and p(GMA)-*b*-p(Alkyl-TAFMA-*co*-RhMA) – were synthesized from the hydrophilic p(GMA) mCTA using RAFT polymerization (**Figure 2A**). The synthesis of p(GMA) mCTA is shown in **Figure 2A**. GMA was chosen due to its relatively low molecular weight (MW, 160.2 Da) which subsequently increased

TAF wt% in the synthesized drugamers. The relatively short p(GMA) mCTA with chain end fidelity was successfully synthesized by using the feeding molar ratio of [GMA]:[CTA]:[AIBN]=50/1/0.05 and allowing 59% monomer conversion. ^{1}H NMR spectrum shows characteristic peaks of pGMA mCTA (**Figure S6**). MW and MW distribution of p(GMA) mCTA were determined using SEC (absolute M_n=7,500 Da, M_w/M_n=1.14, shown in **Table 1**: Entry 1). The unimodal MW distribution of p(GMA) was also observed (**Figure 3**).

The synthetic conditions of the diblock drugamers were first optimized with the Benzyl-TAFMA in order to achieve high monomer conversion. The polymerization at 60 °C using an optimal feeding molar ratio of [Benzyl-TAFMA]:[p(GMA) mCTA]:[AIBN]=12/1/0.06 allowed 98% monomer conversion after 7.5 h. The TAF wt% was 34% based on ^{1}H NMR calculation (shown in **Table 1**: Entry 2, and **Figure S7**). The absolute MW and MW distributions of p(GMA)-*b*-p(Benzyl-TAFMA) were determined using SEC (M_n=19,750 Da, M_w/M_n=1.16, shown in **Table 1**: Entry 2). **Figure 3** shows that the SEC trace of p(GMA)-*b*-p(Benzyl-TAFMA) shifted towards higher MW (lower elution time) as compared to that of p(GMA) mCTA suggesting successful chain extension of p(GMA) mCTA with Benzyl-TAFMA.

The synthesis of p(GMA)-*b*-p(Alkyl-TAFMA-*co*-RhMA) was carried out in the same conditions as described for p(GMA)-*b*-p(Benzyl-TAFMA). The addition of RhMA enables the visualization of the depot using IVIS. The feeding molar ratio of [Alkyl-TAFMA]:[RhMA] was 21/1.5 ensuring the conjugation of at least one RhMA per polymer chain (**Table 1**: Entry 3). The TAF wt% and theoretical MW were 51% and 21,000 Da, respectively, as determined by ^{1}H NMR (**Table 1**: Entry 3, and **Figure S8**). Absolute MW of the polymer could not be determined by SEC due to the interference of rhodamine with light scattering detector.

Table 1. Summary of feeding molar ratio, monomer conversion, molecular weight, molecular mass dispersity, monomer wt% and TAF wt% in each polymer reported in this study.

Entry	Polymer	[M]:[CTA]:[I]	Monomer Conversion [a] (%)	M_n [b] (Da)	M_w/M_n	GMA monomer wt% [a,d]	TAF monomer wt% [a,d]	Drug wt% [a]
1	p(GMA) mCTA	50/1/0.05	59	7,500	1.14	100	0	-
2	p(GMA)-*b*-p(Benzyl-TAFMA)	12/1/0.06	98	19,750	1.16	39.4	60.6	34
3	p(GMA)-*b*-p(Alkyl-TAFMA-*co*-RhMA)	22.5/1/0.075	95	21,000[c]	-	32.7	67.3	51
4	p(Benzyl-TAFMA-*co*-RhMA)	12/1/0.1	89	9,100[c]	-	0	95.9	54.5
5	p(Alkyl-TAFMA-*co*-RhMA)	16/1/0.05	80	8,400[c]	-	0	96.9	73

[M] – feeding monomer molar, [CTA] – feeding chain transfer agent molar, [I] – feeding initiator molar
[a]As determined by ^{1}H NMR spectroscopy
[b]As determined by SEC
[c]As calculated based on the monomer conversion determined by ^{1}H NMR spectroscopy. The absolute MWs of these polymers cannot be determined by SEC due to the interference of rhodamine with light scattering detector.
[d]RhMA was not considered in GMA and TAF monomer wt% calculation due to its low polymerization degree (DP=1)

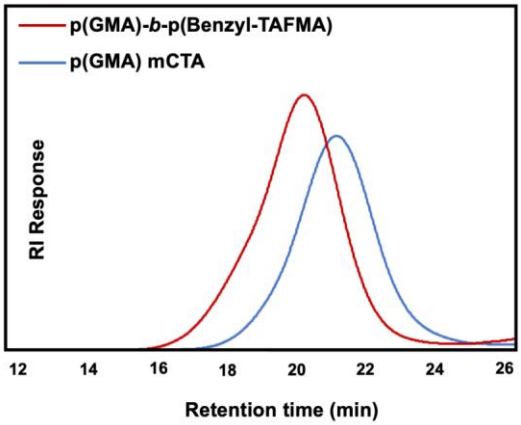

Figure 3. SEC traces of p(GMA) mCTA (**Table 1:** Entry 1) and p(GMA)-*b*-p(Benzyl-TAFMA) (**Table 1:** Entry 2).

3.2.2. Synthesis of homo TAF drugamers

The homopolymers were synthesized to maximize the TAF wt%. The p(Benzyl-TAFMA-*co*-RhMA) and p(Alkyl-TAFMA-*co*-RhMA) were synthesized by RAFT copolymerization of drug monomer and RhMA. The reactions were activated using the CTA (ECT) and an initiator (AIBN or V70) and carried out in DMF at 60 °C under nitrogen atmosphere (**Figure 2B**). The targeted degree polymerization (DP) of RhMA was one to enable the visualization of depot using IVIS. The TAF wt% were 54.5% and 73% for p(Benzyl-TAFMA-*co*-RhMA) and p(Alkyl-TAFMA-*co*-RhMA), respectively (**Table 1**: Entry 4, Entry 5; and **Figure S10**, **Figure S12**). The absolute MW of these polymers could not be determined by SEC due to the interference of RhMA with light scattering detector. The approximate MW values were determined using the monomer conversion (**Table 1**: Entry 4, Entry 5).

3.3. Storage stability of the TAF diblock p(GMA)-*b*-p(Benzyl-TAFMA)

The storage stability of TAF conjugated polymer was evaluated over a 6-month period by characterizing the less stable p(GMA)-*b*-p(Benzyl-TAFMA) diblock polymer in solid form in an accelerated degradation study. The stability/degradation was determined by HPLC and ^{1}H NMR spectroscopy. ^{1}H NMR signals at 8.10 and 8.13 ppm started to appear after three weeks, corresponding to purine ring protons of TAF not bound to polymer backbone (**Figure S13**). HPLC and ^{1}H NMR analysis showed 3.5% and 5.5% TAF release from the parent polymer over the 6-month period, respectively (**Figure 4**, **Figure S13**). Although this small amount of TAF was released, no further degradation of TAF was observed within the detection limits. The remarkable stability (≈95 %) of TAF on the polymer backbone under accelerated degradation conditions

suggests that the depot could be stored for significant time periods without cold chain in this lyophilized state prior to solubilization and injection.

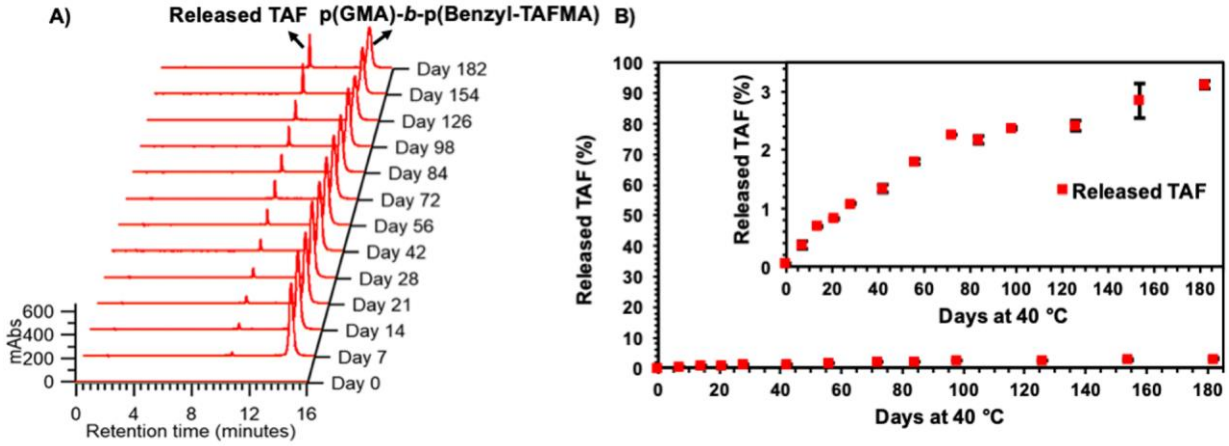

Figure 4. HPLC analysis of thermal accelerated degradation of p(GMA)-*b*-p(Benzyl-TAFMA) at 40 ± 2 °C: (**A**) UV chromatograms of p(GMA)-*b*-p(Benzyl-TAFMA) samples post-incubation at designated time points from 0 – 180 days showing polymer and TAF peaks at 14.8 and 10.7 min, respectively; (**B**) Percentage of released TAF from the polymer (as calculated by equation I) at designated time points from 0 – 180 days.

3.4. Validation of TAF metabolism in mouse model for long-acting HIV PrEP development

3.4.1. Metabolites of TAF after intravenous entry into the mouse blood compartment

The metabolism of TAF in the mouse model has not been widely investigated and reported. Given that the mouse model would offer higher throughput in developing new long-acting HIV PrEP products, we have characterized the key metabolites needed to assess depots after subcutaneous injection. The injection of TAF directly into the blood mimicked the entry of parent TAF into the blood of the mouse from the subcutaneous compartment. Prior work has not clearly distinguished TAF metabolism in the blood from that occurring in the subcutaneous compartment.

Hence, we first studied the metabolites of TAF in blood compartment by intravenously administering TAF at the dose of 45 mg/kg. LC-MS/MS results showed that TAF was rapidly metabolized and could not be detected in mouse plasma at any time point studied.[50] Unlike metabolism reported in humans and canines,[50] we found that the metabolite TAF-alanine was detected at a significantly high signal at the early time point (5 min) after injection (**Figure S14**). The more stable metabolite TFV was also detected and could be better quantitated with higher levels throughout the 8h study (**Figure 5A**). TFV-DP is a critical metabolite of TAF produced after intracellular processing in PBMC, used to assess whether clinically relevant levels of this active drug species are achieved to correlate with likely PrEP efficacy.[51–54] To our knowledge, TAF

metabolism to this metabolite has not been previously reported in the mouse model. We isolated PBMC and quantified the TFV-DP levels. **Figure 5B** shows that TFV-DP could be detected and well quantified at all time points throughout the study. A control injection of TFV into blood did not result in quantifiable TFV-DP, demonstrating that the presence of this metabolite is also a marker of parent drug TAF reaching the blood compartment after subcutaneous depot formation.

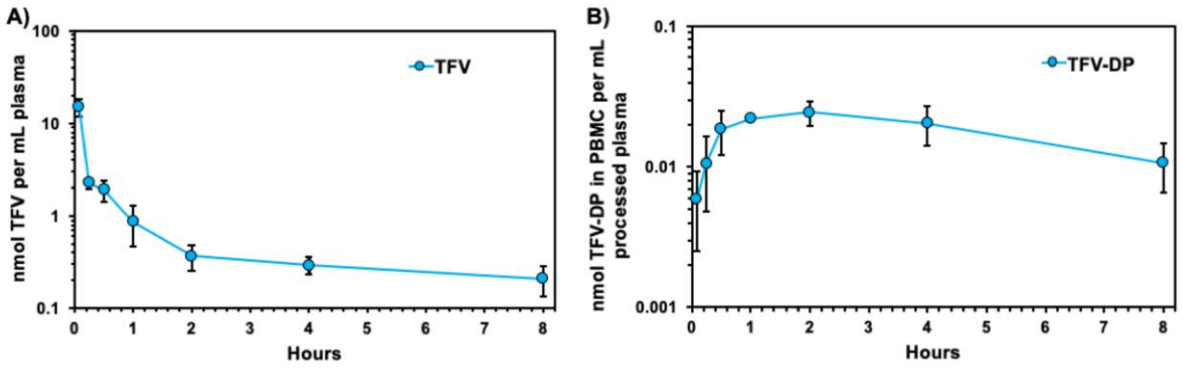

Figure 5. Metabolism of TAF in an intravenous mouse model after a single dose of 45 mg/kg TAF prepared in 5% dextrose solution. The PK profiles of (**A**) TFV in plasma (nmol per mL plasma) and (**B**) TFV-DP in PBMC (nmol per mL processed plasma) were analyzed using LC-MS/MS. Each data point represents the means ± standard deviations from three mice.

3.4.2. Metabolites of TAF from injection in the subcutaneous mouse compartment

For subcutaneous implant and injectable depot development, the metabolism in this compartment is also important background to interpret delivery properties. Unlike TAF injected directly into the blood, TAF could be quantified after subcutaneous injection in this compartment (**Figure 6A**). TAF was converted to TFV whose concentrations were immediately significant at 5 min post-injection (**Figure 6B**). The concentrations of both skin TAF and TFV concentrations dropped exponentially after 2 h post-injection. The low and longer term levels of TAF and TFV in the subcutaneous compartment were likely due to the hydrophobicity of TAF molecules (log P = 1.6) causing a small fraction of aggregated depot formation after being subcutaneously deposited.

The injection of TAF in the subcutaneous compartment did not lead to measurable TAF levels in the blood compartment and did not maintain the TFV levels in plasma. The maximum plasma TFV concentrations were recorded at 2 h, which dramatically decreased after 4 h and thereafter likely due to the small level coming from the aggregated depot (**Figure 6C**). A key finding was that the intracellular PBMC compartment biomarker TFV-DP could be measured after pooling of PBMC from 3 mice. This indicated that TAF could reach and enter the PBMC compartment as a

pulse after subcutaneous injection. The pooled concentrations were >5000 fmol per 10^6 PBMC and ~1200 fmol per 10^6 PBMC at 8 h and 2 d, respectively (**Figure 6D**).

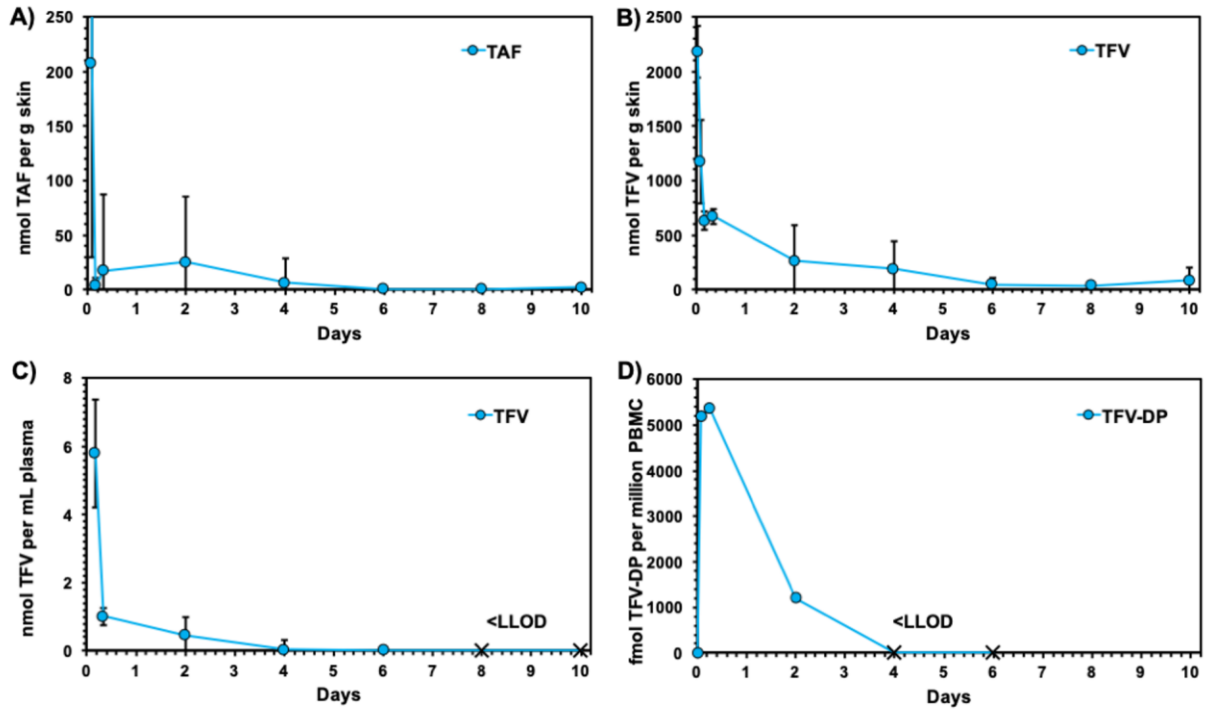

Figure 6. Metabolism of TAF in a subcutaneous mouse model after a single dose of 6.77 mg/mouse TAF prepared in a mixture of ultrapure water, USP grade propylene glycol and benzyl alcohol (4:5:1 *v/v*). The PK profiles of (**A**) TAF in skin (nmol per g skin); (**B**) TFV in skin (nmol per g skin); (**C**) TFV in plasma (nmol per mL plasma); and (**D**) TFV-DP in PBMC (fmol per million PBMC, PBMC were collected from 3 mice and pooled together for the analysis thus not presented as ± standard deviation) were analyzed using LC-MS/MS. Each data point represents the means ± standard deviations from three mice.

In conclusion, these metabolite and PK studies provide the key background to interpret the following drugamer depot results in skin and plasma. The rapid disappearance of TAF in blood means that any TAF seen from candidate depots in the blood must be continuously produced as parent drug released from the depot. This can be confirmed by the presence of TFV-DP in the PBMC compartment which again requires parent TAF to be entering the blood since TFV does not give rise to significant TFV-DP in the PBMC compartment.

3.5. Characterization of TAF depot sustained release performance

3.5.1. Tolerability at injection Site

The tolerability at injection site of TAF drugamer depot was assessed after a 60-day period by evaluating H&E images of the explanted skin cross-sectioned tissues carrying the p(Alkyl-TAFMA-*co*-RhMA) depot formulated in DMSO. The H&E images of the explanted skin cross-

sectioned tissues collected at day 60 from mice received DMSO vehicle were used as controls. In comparison to controls, there was only minimal plasmacytic, lymphocytic and neutrophilic inflammation in the tissue surrounding the subcutaneous p(Alkyl-TAFMA-*co*-RhMA) depot showing its good biocompatibility (representative H&E images of the explanted skin cross-sectioned tissues are shown in **Figure S18**).

3.5.2. Depot performance of diblock TAF drugamers

The diblock polymer architecture was first tested as a long-acting, subcutaneous injection depot. The PK of TAF and TFV metabolites were characterized in explanted skin and plasma. Diblock copolymers with the common hydrophilic, low MW GMA first block segment were compared with either the faster degrading benzylic linker design versus slower degrading alkyl linker design: p(GMA)-*b*-p(Benzyl-TAFMA) and p(GMA)-*b*-p(Alkyl-TAFMA). The influence of the linker can be clearly observed in the PK plots in skin and plasma. The faster degrading Benzyl-TAFMA design showed higher levels of drug release in both compartments, and as a result did not sustain release over 10 days into the blood (**Figure 7A)**. The slower releasing Alkyl-TAFMA design showed sustained release over a full 50-day time period in skin and in plasma compartments.

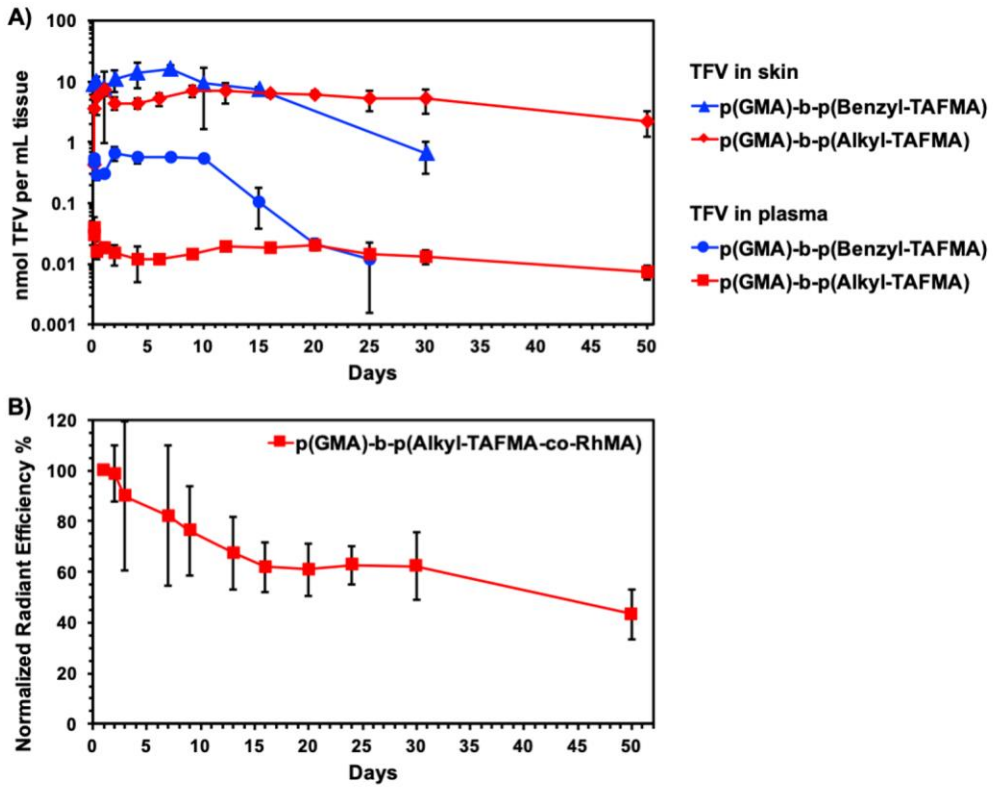

Figure 7. (**A**) Following a single subcutaneous injection of p(GMA)-*b*-p(Benzyl-TAFMA) or p(GMA)-*b*-p(Alkyl-TAFMA) prepared in a mixture of ultrapure water, USP grade propylene glycol and benzyl alcohol (4:5:1 *v/v*) at the dose of equivalent TAF 6.77 mg/mouse, the PK profiles of TFV in skin (nmol per g skin) and TFV in plasma (nmol per mL plasma) were analyzed using LC-MS/MS. (**B**) Following a single subcutaneous injection of p(GMA)-*b*-p(Alkyl-TAFMA-*co*-RhMA) prepared in a mixture of ultrapure water, USP grade propylene glycol and benzyl alcohol (4:5:1 *v/v*) at the dose of equivalent TAF 6.77 mg/mouse, the fluorescent intensity emitted from the depot was normalized as radiant efficiency percentage using equation II to estimate the dissolution and clearance rates of the polymer. Each data point represents the means ± standard deviations from at least three mice.

The depot degradation kinetics were assessed by imaging rhodamine-labeled polymers by IVIS (**Figure 7B**, **Figure S16)**. The release kinetics of TAF from the depot were generally also well correlated with the dissolution of the depot as measured in the decrease of the fluorescent radiant efficiency over time (**Figure 7B**). The p(GMA)-*b*-p(Benzyl-TAFMA) depots showed a faster dissolution rate compared to the slower releasing p(GMA)-*b*-p(Alkyl-TAFMA) depots, connecting depot dissolution to the mechanistic release of TAF and corresponding loss of hydrophobicity through hydrolysis/enzymatic conversion to hydrophilic chains.

3.5.3. Depot performance of homopolymer TAF depot designs

The homopolymer depots were designed to maximize TAF drug wt% and as a result to maximize the potential duration of the long-acting depot. As homopolymer segments, their MW

was also kept low to promote renal clearance after TAF release. The p(Benzyl-TAFMA) depot achieves 54.5 drug wt% and the p(Alkyl-TAFMA) depot achieves 73 drug wt% at starting MWs of 9,100 Da and 8,400 Da, respectively (lower MWs after drug release and dissolution from depot). The homopolymers could be formulated in DMSO with high solubility of >700 mg/mL. Together the high drug wt% and solubility yields long-acting depots having enough TAF to deliver over many months to years time frame at target levels around 1 mg/day.[22,26,55] The homopolymer depots also formed tighter and less spread depots upon injection compared to the diblock depot formulations (**Figure 8C, Figure S16**).

As expected, the faster releasing p(Benzyl-TAFMA) showed a higher dosing level in the blood compartment compared to the p(Alkyl-TAFMA), again showing the tunability of depot PK with linker choice (**Figure 8A**). TAF was not observable in the blood for injected parent drug (IV or subcutaneous), either of the diblock polymer depots, or the p(Benzyl-TAFMA) homopolymer depot design. However, for the first time in mouse, the parent TAF drug was observed with a sustained release profile along with TFV. The p(Alkyl-TAFMA) depot was characterized in a 60-day study and showed a zero-order, steady plasma TAF and TFV profile over the 60 days (**Figure 8A**). The molar ratios of plasma TAF:TFV concentrations were 0.52 ± 0.18 (mean ± SD) and relatively stable throughout the 60-day study. These results demonstrate that TAF is being released as the parent drug from the depot over the two-month study period.[56,57] As shown in **Figure 8C**, some remaining p(Alkyl-TAFMA-*co*-RhMA) depot could still be observed at the end of the 60-day study, suggesting longer release periods were possible.

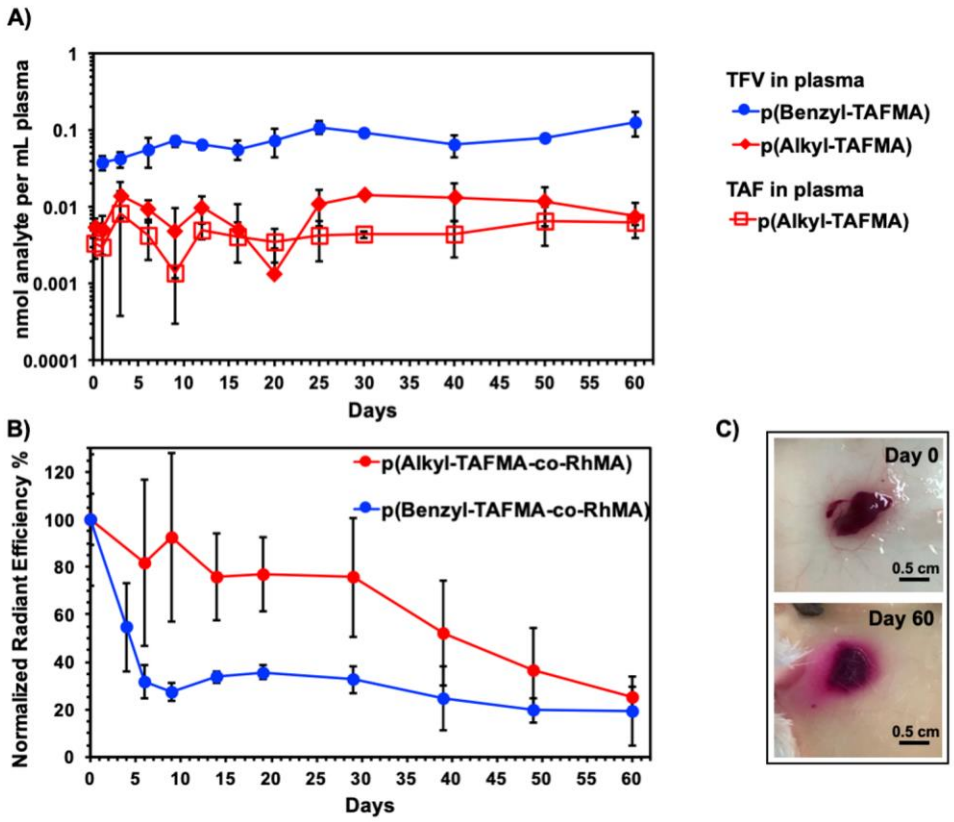

Figure 8. (A) Following a single subcutaneous injection of p(Benzyl-TAFMA) or p(Alkyl-TAFMA) prepared in DMSO at the dose of equivalent TAF 6.77 mg/mouse, the PK profiles of TFV in plasma (nmol per mL plasma) and TAF in plasma (nmol per mL plasma) were analyzed using LC-MS/MS. (**B**) Following a single subcutaneous injection of p(Benzyl-TAFMA-*co*-RhMA) or p(Alkyl-TAFMA-*co*-RhMA) prepared in DMSO at the dose of equivalent TAF 6.77 mg/mouse, the fluorescent intensity emitted from the depot was normalized as radiant efficiency percentage using equation II to estimate the dissolution and clearance rates of the polymer. Each data point represents the means ± standard deviations from at least three mice. (**C**) Pictures of p(Alkyl-TAFMA-*co*-RhMA) subcutaneous depot at day 0 and day 60 post-injection.

The most important predictor of TAF long-acting prophylaxis is the TFV-DP metabolite and biomarker level in the PBMC compartment.[51–54] Both the p(Alkyl-TAFMA) and the p(Benzyl-TAFMA) homopolymer depots yield high levels of TFV-DP in the PBMC compartment (**Figure 9**). It is worth noted that the PBMC in this study were cryopreserved prior to analysis, which might lead to 33 to 67% loss of TFV-DP.[26] The p(Benzyl-TAFMA) showed higher initial levels of TFV-DP in PBMC consistent with the higher levels of the plasma TFV metabolite. The level of TFV-DP shows a sharper drop-off in its PK profile, however, and the depot itself shows a similar faster degradation in the IVIS imaging characterization (**Figure 8B**). The p(Alkyl-TAFMA) shows a steadier profile of TFV-DP in the PBMC compartment (**Figure 9**), consistent with its lower and more consistent TAF/TFV profile, and with its more linear depot degradation profile by IVIS

imaging (**Figure 8A,B**). The MW of the starting homopolymers are below 10,000 Da with all of the drug incorporated, and the smaller p(Alkyl-TAFMA-*co*-RhMA) chains released from the depot after drug release were imaged by IVIS in brain, liver, lungs, heart, kidneys and spleen. As expected, these small chains were primarily eliminated via the kidneys over the study period (**Figure S17**).

It was surprising that p(Benzyl-TAFMA) showed such a high level of TFV-DP in the PBMC compartment, given that no TAF could be observed in blood. The parent TAF drug also showed this profile with no observable TAF in the blood at our earliest time point of 5 min, yet there was TFV-DP detectable in the PBMCs. These results suggest that the kinetics of TAF entry into PBMC after entry of the drug from the subcutaneous compartment into the blood must be faster than TAF metabolism and disappearance in the mouse model. The p(Alkyl-TAFMA) depot showed a steadier release of both TAF and TFV, along with a steadier profile of depot degradation and the TFV-DP metabolite in PBMC. Clinical trials have suggested that the TFV-DP at a minimum concentration of 24 fmol per 10^6 PBMC provides 90% protection in HIV iPrEX.[58] In this study, the average TFV-DP concentrations achieved by the polymer depots are at least 10-fold higher than the minimally protective concentration from iPrEX.

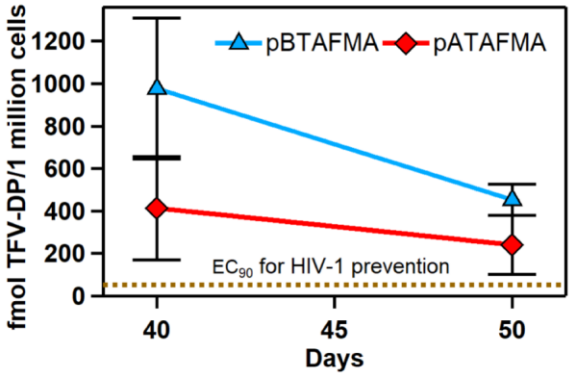

Figure 9. TFV-DP concentrations per million PBMC after 50 d of a single subcutaneous injection of either p(Benzyl-TAFMA) or p(Alkyl-TAFMA). All data point represents the means ± standard deviations from three mice.

4. Conclusion

In this study, we have demonstrated that injectable subcutaneous depots based on the drugamer platform sustain the release of TAF over 60-day periods, with loading of the key TFV-DP metabolite at high levels in the PBMC compartment. This injectable depot is a simple polymer in a formulation solvent. The polymers can be architectured as block copolymers or homopolymers,

and we show that different linkers can be used to tune the PK profiles. As a prodrug approach, the depots do not exhibit significant early stage burst release. The depot release was steady over the two month period characterized, and current studies were not long enough to definitively study the end-stage. After drug release and pendant linker degradation, the hydrophilic backbone chains are very low MW and were shown to clear renally in the case of the homopolymer depot designs. This mechanism could potentially clear any chains still containing unreleased drugs to prevent a late-stage burst phase, though this will require longer studies to confirm. By polymerizing pre-synthesized prodrug monomers, the depots achieve high drug weight percentages, which can translate to higher drug sink and longer release durations, and lower volumes of administration. These high drug weight percentages also suggest that combination drugs could be copolymerized into depots while maintaining significant drug sinks of each. We anticipate this platform can be tailored to a variety of ARV combinations for therapy and prophylaxis, and with its high intrinsic storage stability could be developed toward future global health and infectious disease settings.

5. Acknowledgements

This work was supported by the Bill & Melinda Gates Foundation, grant agreement number OPP1156518. Almar Postma acknowledges CSIRO for a Julius Career Award. We dedicate this paper to Professor Kopecek and his remarkable contributions to the field of drug delivery, to polymer therapeutics which underlie this work, and finally for his even more remarkable friendship and inspiring spirit that has enlivened our group over the past three decades.

6. Competing financial interests

The authors declare no competing financial interests.

7. Supporting information

Supporting information is available online.

8. References

[1] R.M. Grant, J.R. Lama, P.L. Anderson, V. McMahan, A.Y. Liu, L. Vargas, P. Goicochea, M. Casapía, J.V. Guanira-Carranza, M.E. Ramirez-Cardich, O. Montoya-Herrera, T. Fernández, V.G. Veloso, S.P. Buchbinder, S. Chariyalertsak, M.S. Chariyalertsak, L.G. Bekker, K.H. Mayer, E.G. Kallás, K.R. Amico, K. Mulligan, L.R. Bushma, R.J. Hance, C. Ganoza, P. Defechereux, B. Postle, F. Wang, J. McConnell, J.H. Zheng, J. Lee, J.F. Rooney, H.S. Jaff, A.I. Martinez, D.N. Burns, D. V. Glidden, Preexposure chemoprophylaxis for HIV prevention in men who have sex with men, N. Engl. J. Med. 363 (2010) 2587–2599. doi:10.1056/NEJMoa1011205.

[2] M.C. Thigpen, P.M. Kebaabetswe, L.A. Paxton, D.K. Smith, C.E. Rose, T.M. Segolodi, F.L. Henderson, S.R. Pathak, F.A. Soud, K.L. Chillag, R. Mutanhaurwa, L.I. Chirwa, M. Kasonde, D. Abebe, E. Buliva, R.J. Gvetadze, S. Johnson, T. Sukalac, V.T. Thomas, C. Hart, J.A. Johnson, C.K. Malotte, C.W. Hendrix, J.T. Brooks, Antiretroviral preexposure prophylaxis for heterosexual HIV transmission in Botswana, N. Engl. J. Med. 367 (2012) 423–434. doi:10.1056/NEJMoa1110711.

[3] K. Choopanya, M. Martin, P. Suntharasamai, U. Sangkum, P.A. Mock, M. Leethochawalit, S. Chiamwongpaet, P. Kitisin, P. Natrujirote, S. Kittimunkong, R. Chuachoowong, R.J. Gvetadze, J.M. McNicholl, L.A. Paxton, M.E. Curlin, C.W. Hendrix, S. Vanichseni, Antiretroviral prophylaxis for HIV infection in injecting drug users in Bangkok, Thailand (the Bangkok Tenofovir Study): A randomised, double-blind, placebo-controlled phase 3 trial, Lancet. 381 (2013) 2083–2090. doi:10.1016/S0140-6736(13)61127-7.

[4] K.A. Thomson, J.M. Baeten, N.R. Mugo, L.G. Bekker, C.L. Celum, R. Heffron, Tenofovir-based oral preexposure prophylaxis prevents HIV infection among women, Curr. Opin. HIV AIDS. 11 (2016) 18–26. doi:10.1097/COH.0000000000000207.

[5] L. Van Damme, A. Corneli, K. Ahmed, K. Agot, J. Lombaard, S. Kapiga, M. Malahleha, F. Owino, R. Manongi, J. Onyango, L. Temu, M.C. Monedi, P. Mak'Oketch, M. Makanda, I. Reblin, S.E. Makatu, L. Saylor, H. Kiernan, S. Kirkendale, C. Wong, R. Grant, A. Kashuba, K. Nanda, J. Mandala, K. Fransen, J. Deese, T. Crucitti, T.D. Mastro, D. Taylor, Preexposure prophylaxis for HIV infection among African women, N. Engl. J. Med. 367 (2012) 411–422. doi:10.1056/NEJMoa1202614.

[6] J.M. Marrazzo, G. Ramjee, B.A. Richardson, K. Gomez, N. Mgodi, G. Nair, T. Palanee, C. Nakabiito, A. Van Der Straten, L. Noguchi, C.W. Hendrix, J.Y. Dai, S. Ganesh, B. Mkhize, M. Taljaard, U.M. Parikh, J. Piper, B. Mâsse, C. Grossman, J. Rooney, J.L. Schwartz, H. Watts, M.A. Marzinke, S.L. Hillier, I.M. McGowan, Z.M. Chirenje, Tenofovir-based preexposure prophylaxis for HIV infection among African women, N. Engl. J. Med. 372 (2015) 509–518. doi:10.1056/NEJMoa1402269.

[7] W.R. Lykins, E. Luecke, D. Johengen, A. van der Straten, T.A. Desai, Long acting systemic HIV pre-exposure prophylaxis: an examination of the field, Drug Deliv. Transl. Res. 7 (2017) 805–816. doi:10.1007/s13346-017-0391-6.

[8] K. Singh, S.G. Sarafianos, A. Sönnerborg, Long-acting Anti-HIV drugs targeting HIV-1 reverse transcriptase and integrase, Pharmaceuticals. 12 (2019). doi:10.3390/ph12020062.

[9] E.D. Weld, C. Flexner, Long-acting implants to treat and prevent HIV infection, Curr. Opin. HIV AIDS. 15 (2020) 33–41. doi:10.1097/COH.0000000000000591.

[10] D.H. Surve, A.B. Jindal, Recent advances in long-acting nanoformulations for delivery of

antiretroviral drugs, J. Control. Release. 324 (2020) 379–404. doi:10.1016/j.jconrel.2020.05.022.

[11] R.J. Landovitz, S. Li, B. Grinsztejn, H. Dawood, A.Y. Liu, M. Magnus, M.C. Hosseinipour, R. Panchia, L. Cottle, G. Chau, P. Richardson, M.A. Marzinke, C.W. Hendrix, S.H. Eshleman, Y. Zhang, E. Tolley, J. Sugarman, R. Kofron, A. Adeyeye, D. Burns, A.R. Rinehart, D. Margolis, W.R. Spreen, M.S. Cohen, M. McCauley, J.J. Eron, Safety, tolerability, and pharmacokinetics of long-acting injectable cabotegravir in low-risk HIV-uninfected individuals: HPTN 077, a phase 2a randomized controlled trial, PLoS Med. 15 (2018). doi:10.1371/journal.pmed.1002690.

[12] M.E. Clement, R. Kofron, R.J. Landovitz, Long-acting injectable cabotegravir for the prevention of HIV infection, Curr. Opin. HIV AIDS. 15 (2020) 19–26. doi:10.1097/COH.0000000000000597.

[13] Exciting new results from long-acting PrEP study show it to be effective in preventing HIV acquisition in men who have sex with men and transgender women, World Heal. Organ. (2020). https://www.who.int/news-room/detail/20-05-2020-exciting-new-results-from-long-acting-prep-study-show-it-to-be-effective-in-preventing-hiv-acquisition-in-msm-and-transgender-women (accessed August 12, 2020).

[14] L.G. Bekker, S. Li, S. Pathak, E.E. Tolley, M.A. Marzinke, J.E. Justman, N.M. Mgodi, M. Chirenje, S. Swaminathan, A. Adeyeye, J. Farrior, C.W. Hendrix, E. Piwowar-Manning, P. Richardson, S.H. Eshelman, H. Redinger, P. Williams, N.D. Sista, Safety and tolerability of injectable Rilpivirine LA in HPTN 076: A phase 2 HIV pre-exposure prophylaxis study in women, EClinicalMedicine. 21 (2020). doi:10.1016/j.eclinm.2020.100303.

[15] A. Jackson, I. McGowan, Long-acting rilpivirine for HIV prevention, Curr. Opin. HIV AIDS. 10 (2015) 253–257. doi:10.1097/COH.0000000000000160.

[16] F. Ferretti, M. Boffito, Rilpivirine long-Acting for the prevention and treatment of HIV infection, Curr. Opin. HIV AIDS. 13 (2018) 300–307. doi:10.1097/COH.0000000000000474

[17] S.L. Letendre, A. Mills, D. Hagins, S. Swindells, F. Felizarta, J. Devente, C. Bettacchi, Y. Lou, S. Ford, K. Sutton, J.S. Shaik, H. Crauwels, R. D'Amico, P. Patel, Pharmacokinetics and antiviral activity of cabotegravir and rilpivirine in cerebrospinal fluid following long-acting injectable administration in HIV-infected adults, J. Antimicrob. Chemother. 75 (2020) 648–655. doi:10.1093/jac/dkz504.

[18] D.A. Margolis, J. Gonzalez-Garcia, H.J. Stellbrink, J.J. Eron, Y. Yazdanpanah, D. Podzamczer, T. Lutz, J.B. Angel, G.J. Richmond, B. Clotet, F. Gutierrez, L. Sloan, M.S. Clair, M. Murray, S.L. Ford, J. Mrus, P. Patel, H. Crauwels, S.K. Griffith, K.C. Sutton, D.

Dorey, K.Y. Smith, P.E. Williams, W.R. Spreen, Long-acting intramuscular cabotegravir and rilpivirine in adults with HIV-1 infection (LATTE-2): 96-week results of a randomised, open-label, phase 2b, non-inferiority trial, Lancet. 390 (2017) 1499–1510. doi:10.1016/S0140-6736(17)31917-7.

[19] C. Fernandez, C.L. van Halsema, Evaluating cabotegravir/rilpivirine long-acting, injectable in the treatment of HIV infection: Emerging data and therapeutic potential, HIV/AIDS - Res. Palliat. Care. 11 (2019) 179–192. doi:10.2147/HIV.S184642.

[20] S. Perazzolo, L.M. Shireman, J. Koehn, L.A. McConnachie, J.C. Kraft, D.D. Shen, R.J.Y. Ho, Three HIV Drugs, Atazanavir, Ritonavir, and Tenofovir, Coformulated in Drug-Combination Nanoparticles Exhibit Long-Acting and Lymphocyte-Targeting Properties in Nonhuman Primates, J. Pharm. Sci. 107 (2018) 3153–3162. doi:10.1016/j.xphs.2018.07.032.

[21] P.K. Prathipati, S. Mandal, G. Pon, R. Vivekanandan, C.J. Destache, Pharmacokinetic and Tissue Distribution Profile of Long Acting Tenofovir Alafenamide and Elvitegravir Loaded Nanoparticles in Humanized Mice Model, Pharm. Res. 34 (2017) 2749–2755. doi:10.1007/s11095-017-2255-7.

[22] M. Kovarova, S.R. Benhabbour, I. Massud, R.A. Spagnuolo, B. Skinner, C.E. Baker, C. Sykes, K.R. Mollan, A.D.M. Kashuba, J.G. García-Lerma, R.J. Mumper, J.V. Garcia, Ultra-long-acting removable drug delivery system for HIV treatment and prevention, Nat. Commun. 9 (2018). doi:10.1038/s41467-018-06490-w.

[23] S.R. Benhabbour, M. Kovarova, C. Jones, D.J. Copeland, R. Shrivastava, M.D. Swanson, C. Sykes, P.T. Ho, M.L. Cottrell, A. Sridharan, S.M. Fix, O. Thayer, J.M. Long, D.J. Hazuda, P.A. Dayton, R.J. Mumper, A.D.M. Kashuba, J. Victor Garcia, Ultra-long-acting tunable biodegradable and removable controlled release implants for drug delivery, Nat. Commun. 10 (2019). doi:10.1038/s41467-019-12141-5.

[24] K.M. Luginbuhl, J.L. Schaal, B. Umstead, E.M. Mastria, X. Li, S. Banskota, S. Arnold, M. Feinglos, D. D'Alessio, A. Chilkoti, One-week glucose control via zero-order release kinetics from an injectable depot of glucagon-like peptide-1 fused to a thermosensitive biopolymer, Nat. Biomed. Eng. 1 (2017). doi:10.1038/s41551-017-0078.

[25] S.E. Barrett, R.S. Teller, S.P. Forster, L. Li, M.A. Mackey, D. Skomski, Z. Yang, K.L. Fillgrove, G.J. Doto, S.L. Wood, J. Lebron, J.A. Grobler, R.I. Sanchez, Z. Liu, B. Lu, T. Niu, L. Sun, M.E. Gindy, Extended-duration MK-8591-eluting implant as a candidate for HIV treatment and prevention, Antimicrob. Agents Chemother. 62 (2018) e01058-18. doi:10.1128/AAC.01058-18.

[26] M. Gunawardana, M. Remedios-Chan, C.S. Miller, R. Fanter, F. Yang, M.A. Marzinke,

C.W. Hendrix, M. Beliveau, J.A. Moss, T.J. Smith, M.M. Baum, Pharmacokinetics of long-acting tenofovir alafenamide (GS-7340) subdermal implant for HIV prophylaxis, Antimicrob. Agents Chemother. 59 (2015) 3913–3919. doi:10.1128/AAC.00656-15.

[27] L.M. Johnson, S.A. Krovi, L. Li, N. Girouard, Z.R. Demkovich, D. Myers, B. Creelman, A. van der Straten, Characterization of a reservoir-style implant for sustained release of tenofovir alafenamide (TAF) for HIV pre-exposure prophylaxis (PrEP), Pharmaceutics. 11 (2019). doi:10.3390/pharmaceutics11070315.

[28] C.Y.X. Chua, P. Jain, A. Ballerini, G. Bruno, R.L. Hood, M. Gupte, S. Gao, N. Di Trani, A. Susnjar, K. Shelton, L.R. Bushman, M. Folci, C.S. Filgueira, M.A. Marzinke, P.L. Anderson, M. Hu, P. Nehete, R.C. Arduino, J.K. Sastry, A. Grattoni, Transcutaneously refillable nanofluidic implant achieves sustained level of tenofovir diphosphate for HIV pre-exposure prophylaxis, J. Control. Release. 286 (2018) 315–325. doi:10.1016/j.jconrel.2018.08.010.

[29] J.E.B. John R. Peery, Scott J. Gilbert, Osmotic implant with membrane and membrane retention means, 2001.

[30] F.P. Pons-Faudoa, A. Sizovs, K.A. Shelton, Z. Momin, L.R. Bushman, C.Y.X. Chua, J.E. Nichols, T. Hawkins, J.F. Rooney, M.A. Marzinke, J.T. Kimata, P.L. Anderson, P.N. Nehete, R.C. Arduino, M. Ferrari, K.J. Sastry, A. Grattoni, Preventive efficacy of a tenofovir alafenamide fumarate nanofluidic implant in SHIV-challenged nonhuman primates, bioRxiv. (2020). doi:10.1101/2020.05.13.091694.

[31] F.Y. Su, S. Srinivasan, B. Lee, J. Chen, A.J. Convertine, T.E. West, D.M. Ratner, S.J. Skerrett, P.S. Stayton, Macrophage-targeted drugamers with enzyme-cleavable linkers deliver high intracellular drug dosing and sustained drug pharmacokinetics against alveolar pulmonary infections, J. Control. Release. 287 (2018) 1–11. doi:10.1016/j.jconrel.2018.08.014.

[32] H.B. Kern, S. Srinivasan, A.J. Convertine, D. Hockenbery, O.W. Press, P.S. Stayton, Enzyme-Cleavable Polymeric Micelles for the Intracellular Delivery of Proapoptotic Peptides, Mol. Pharm. 14 (2017) 1450–1459. doi:10.1021/acs.molpharmaceut.6b01178.

[33] D. Das, S. Srinivasan, A.M. Kelly, D.Y. Chiu, B.K. Daugherty, D.M. Ratner, P.S. Stayton, A.J. Convertine, RAFT polymerization of ciprofloxacin prodrug monomers for the controlled intracellular delivery of antibiotics, Polym. Chem. 7 (2016) 826–837. doi:10.1039/c5py01704a.

[34] D. Das, S. Srinivasan, A.M. Kelly, D.Y. Chiu, B.K. Daugherty, D.M. Ratner, P.S. Stayton, A.J. Convertine, RAFT polymerization of ciprofloxacin prodrug monomers for the controlled intracellular delivery of antibiotics, Polym. Chem. 7 (2016) 826–837.

doi:10.1039/C5PY01704A.

[35] K. Park, S. Skidmore, J. Hadar, J. Garner, H. Park, A. Otte, B.K. Soh, G. Yoon, D. Yu, Y. Yun, B.K. Lee, X. Jiang, Y. Wang, Injectable, long-acting PLGA formulations: Analyzing PLGA and understanding microparticle formation, J. Control. Release. 304 (2019) 125–134. doi:10.1016/j.jconrel.2019.05.003.

[36] D.-K. Ho, B.L.B. Nichols, K.J. Edgar, X. Murgia, B. Loretz, C.-M. Lehr, Challenges and strategies in drug delivery systems for treatment of pulmonary infections, Eur. J. Pharm. Biopharm. 144 (2019) 110–124. doi:10.1016/j.ejpb.2019.09.002.

[37] D. Das, J. Chen, S. Srinivasan, A.M. Kelly, B. Lee, H.N. Son, F. Radella, T.E. West, D.M. Ratner, A.J. Convertine, S.J. Skerrett, P.S. Stayton, Synthetic Macromolecular Antibiotic Platform for Inhalable Therapy against Aerosolized Intracellular Alveolar Infections, Mol. Pharm. 14 (2017) 1988–1997. doi:10.1021/acs.molpharmaceut.7b00093.

[38] M. Danial, S. Telwatte, D. Tyssen, S. Cosson, G. Tachedjian, G. Moad, A. Postma, Combination anti-HIV therapy: Via tandem release of prodrugs from macromolecular carriers, Polym. Chem. 7 (2016) 7477–7487. doi:10.1039/c6py01882c.

[39] P.J. Ruane, E. Dejesus, D. Berger, M. Markowitz, U.F. Bredeek, C. Callebaut, L. Zhong, S. Ramanathan, M. S. Rhee, M.W. Fordyce, K. Yale, Antiviral activity, safety, and pharmacokinetics/pharmacodynamics of tenofovir alafenamide as 10-day monotherapy in HIV-1-positive adults, J. Acquir. Immune Defic. Syndr., 63 (2013) 449–455. doi:10.1097/QAI.0b013e3182965d45.

[40] M. Markowitz, A. Zolopa, K. Squires, P. Ruane, D. Coakley, B. Kearney, L. Zhong, M. Wulfsohn, M.D. Miller, W.A. Lee, Phase I/II study of the pharmacokinetics, safety and antiretroviral activity of tenofovir alafenamide, a new prodrug of the hiv reverse transcriptase inhibitor tenofovir, in HIV-infected adults, J. Antimicrob. Chemother. 69 (2014) 1362–1369. doi:10.1093/jac/dkt532.

[41] S. Mandal, G. Kang, P.K. Prathipati, Y. Zhou, W. Fan, Q. Li, C.J. Destache, Nanoencapsulation introduces long-acting phenomenon to tenofovir alafenamide and emtricitabine drug combination: A comparative pre-exposure prophylaxis efficacy study against HIV-1 vaginal transmission, J. Control. Release. 294 (2019) 216–225. doi:10.1016/j.jconrel.2018.12.027.

[42] S. Mandal, P.K. Prathipati, G. Kang, Y. Zhou, Z. Yuan, W. Fan, Q. Li, C.J. Destache, Tenofovir alafenamide and elvitegravir loaded nanoparticles for long-acting prevention of HIV-1 vaginal transmission, AIDS. 31 (2017) 469–476. doi:10.1097/QAD.0000000000001349.

[43] J. Chen, H.N. Son, J.J. Hill, S. Srinivasan, F.Y. Su, P.S. Stayton, A.J. Convertine, D.M.

Ratner, Nanostructured glycopolymer augmented liposomes to elucidate carbohydrate-mediated targeting, Nanomedicine Nanotechnology, Biol. Med. 12 (2016) 2031–2041. doi:10.1016/j.nano.2016.05.001.

[44] H.N. Son, S. Srinivasan, J.Y. Yhee, D. Das, B.K. Daugherty, G.Y. Berguig, V.G. Oehle, S.H. Kim, K. Kim, I.C. Kwon, P.S. Stayton, A.J. Convertine, Chemotherapeutic copolymers prepared: Via the RAFT polymerization of prodrug monomers, Polym. Chem. 7 (2016) 4494–4505. doi:10.1039/c6py00756b.

[45] P. Zhang, J. Li, M. Ghazwani, W. Zhao, Y. Huang, X. Zhang, R. Venkataramanan, S. Li, Effective co-delivery of doxorubicin and dasatinib using a PEG-Fmoc nanocarrier for combination cancer chemotherapy, Biomaterials. 67 (2015) 104–114. doi:10.1016/j.biomaterials.2015.07.027.

[46] B.E. Watkins, J.S. Kiely, H. Rapoport, Synthesis of Oligodeoxyribonucleotides Using N-Benzyloxycarbonyl-Blocked Nucleosides, J. Am. Chem. Soc. 104 (1982) 5702–5708. doi:10.1021/ja00385a026.

[47] A.K. Saha, P. Schultz, H. Rapoport, 1,1’-Carbonylbis(3-methylimidazolium) Triflate: An Efficient Reagent for Aminoacylations, J. Am. Chem. Soc. 111 (1989) 4856–4859. doi:10.1021/ja00195a043.

[48] J. Noh, B. Kwon, E. Han, M. Park, W. Yang, W. Cho, W. Yoo, G. Khang, D. Lee, Amplification of oxidative stress by a dual stimuli-responsive hybrid drug enhances cancer cell death, Nat. Commun. 6 (2015). doi:10.1038/ncomms7907.

[49] R.B. Greenwald, A. Pendri, C.D. Conover, H. Zhao, Y.H. Choe, A. Martinez, K. Shum, S. Guan, Drug delivery systems employing 1,4- or 1,6-elimination: Poly(ethylene glycol) prodrugs of amine-containing compounds, J. Med. Chem. 42 (1999) 3657–3667. doi:10.1021/jm990166e.

[50] M.A.M. Teresa L. Parsons, Kevin N. Gwenden, Inter-species Differences in Tenofovir Alafenamide Fumarate Stability in Plasma, Antimicrob. Agents Chemother. (2020) 1–10. doi:10.1128/AAC.00930-20.

[51] N.A. Louissaint, Y.J. Cao, P.L. Skipper, R.G. Liberman, S.R. Tannenbaum, S. Nimmagadda, J.R. Anderson, S. Everts, R. Bakshi, E.J. Fuchs, C.W. Hendrix, Single dose pharmacokinetics of oral tenofovir in plasma, peripheral blood mononuclear cells, colonic tissue, and vaginal tissue, AIDS Res. Hum. Retroviruses. 29 (2013) 1443–1450. doi:10.1089/aid.2013.0044.

[52] Guidance for Industry Bioanalytical Method Validation, Vet. Med. (2001).

[53] K.B. Patterson, H.A. Prince, E. Kraft, A.J. Jenkins, N.J. Shaheen, J.F. Rooney, M.S. Cohen, A.D.M. Kashuba, Penetration of tenofovir and emtricitabine in mucosal tissues:

implications for prevention of HIV-1 transmission., Sci. Transl. Med. 3 (2011) 112re4. doi:10.1126/scitranslmed.3003174

[54] C.W. Hendrix, Exploring concentration response in HIV pre-exposure prophylaxis to optimize clinical care and trial design, Cell. 155 (2013) 515-518. doi:10.1016/j.cell.2013.09.030.

[55] J.T. Su, S.M. Simpson, S. Sung, E.B. Tfaily, R. Veazey, M. Marzinke, J. Qiu, D. Watrous, L. Widanapathirana, E. Pearson, M.M. Peet, D. Karunakaran, B. Grasperge, G. Dobek, C.M. Cain, T. Hope, P.F. Kiser, A subcutaneous implant of tenofovir alafenamide fumarate causes local inflammation and tissue necrosis in rabbits and macaques, Antimicrob. Agents Chemother. 64 (2020) e01893-19. doi:10.1128/AAC.01893-19.

[56] P.L. Anderson, J.J. Kiser, E.M. Gardner, J.E. Rower, A. Meditz, R.M. Grant, Pharmacological considerations for tenofovir and emtricitabine to prevent HIV infection, J. Antimicrob. Chemother. 66 (2011) 240–250. doi:10.1093/jac/dkq447.

[57] O. Kis, K. Robillard, G.N.Y. Chan, R. Bendayan, The complexities of antiretroviral drug-drug interactions: role of ABC and SLC transporters, Trends Pharmacol. Sci. 31 (2010) 22–35. doi:10.1016/j.tips.2009.10.001.

[58] P.L. Anderson, D. V. Glidden, A. Liu, S. Buchbinder, J.R. Lama, J.V. Guanira, V. McMahan, L.R. Bushman, M. Casapía, O. Montoya-Herrera, V.G. Veloso, K.H. Mayer, S. Chariyalertsak, M. Schechter, L.G. Bekker, E.G. Kallás, R.M. Grant, Emtricitabine-tenofovir concentrations and pre-exposure prophylaxis efficacy in men who have sex with men, Sci. Transl. Med. 4 (2012) 151ra125. doi:10.1126/scitranslmed.3004006.